Carbon 105 (2016) 544–550

Contents lists available at ScienceDirect

Carbon

journal homepage: www.elsevier.com/locate/carbon

# Transport properties in aggregates of Nb nanowires templated by carbon nanotube films

M. Salvato [a, b, *], C. Cirillo [b, c], R. Fittipaldi [b, c], S.L. Prischepa [d], A. Vecchione [b, c], F. De Nicola [a, e], P. Castrucci [a, e], M. De Crescenzi [a, e], M. Scarselli [a, e], C. Attanasio [c, b]

[a] Dipartimento di Fisica, Università di Roma "Tor Vergata", I-00133, Roma, Italy
[b] CNR-SPIN Salerno, Via Giovanni Paolo II 132, I-84084, Fisciano, Italy
[c] Dipartimento di Fisica "E.R. Caianiello", Università degli Studi di Salerno, Via Giovanni Paolo II 132, I-84084, Fisciano, Italy
[d] Belarusian State University of Informatics and RadioElectronics, 220013, Minsk, Belarus
[e] INFN, Università di Roma "Tor Vergata", I-00133, Roma, Italy

ARTICLE INFO

*Article history:*
Received 3 February 2016
Received in revised form
18 April 2016
Accepted 26 April 2016
Available online 27 April 2016

ABSTRACT

Films of multiwall carbon nanotubes (CNTs), arranged on $Si/SiO_2$ substrates, are used as templates for Nb films with thickness in the range 3–50 nm deposited by sputtering. The resulting aggregates show normal state and superconducting properties similar to those observed in networks of superconducting nanowires (SNW) obtained by other methods. Decreasing the Nb thickness, when the normal state resistance becomes larger than the quantum resistance, a superconductor-insulator transition is observed. Moreover, thermally activated phase slips in thicker samples, evolving in quantum phase slips in thinner nanowires, are observed in the superconducting state. The experimental results indicate that the template method based on CNTs is a promising alternative to the much more expensive nanolithography techniques for obtaining SNWs. Even more important, they indicate CNT films as versatile elements in nanostructured electronic devices.



## 1. Introduction

Carbon nanotubes (CNTs) have been widely studied in the past decade as possible substitutes of Si in electronic systems [1]. In this context, films of CNTs offers interesting perspectives to be used as sensors [2] and photo-conductive based devices [3] in many applications. Moreover, further improvements in their performances were observed after doping [4], functionalizing [5] or simply depositing granular metallic particles on the CNT surface [6]. For this last case, metals deposited on CNTs give rise either to granular structures [7] or to uniform layers [8] depending on the growth techniques and conditions, as well as on the sticking coefficients between the bare CNT surface and the deposited metals. Therefore, since CNTs present a cylindrical shape with a flat surface at atomic level, the deposited metallic layer can inherit their form. In this way, a homogeneous metallic nanowire (NW) with reduced surface roughness can be templated with a thickness that can be easily tuned by changing its deposition time. This characteristic becomes much more intriguing if a superconductor is deposited on a CNT, because a superconducting NW (SNW) can be obtained [9]. However, while it is difficult to process a single carbon nanotube, CNTs can be easily deposited on selected substrates to obtain a rather homogeneous film with controlled thickness that acts as a template for SNW network fabrication. Moreover, at low temperatures, where superconductors work, CNT films are semiconducting or highly resistive with a high thermal conductivity [10], all properties that are essential to avoid current shorts and overheating effects. For these reasons, the use of CNT films, acting as template substrates, seems to be very promising in the fabrication of SNW networks. In this respect, recently, SNWs received a great attention due to their possible use in superconducting electronics [11–17]. The development of high resolution techniques such as electron beam lithography, although expensive, made individual SNWs possible candidates for current standards [11], sensors [12], actuators [13], microwave detectors [14], quantum bits [15–17] and other switching devices based on classical and quantum effects. Recently, the same properties of the individual SNWs have been reported for networks of SNWs [18–20] obtained by etching process as well as by template methods using porous Si or alumina membranes [21–25]. Among the many methods used to fabricate SNWs, the template technique earned a large success since it allows to obtain SNWs by controlling the growth rate in simple deposition

* Corresponding author. Dipartimento di Fisica, Università di Roma "Tor Vergata", I-00133, Roma, Italy.
*E-mail address:* matteo.salvato@roma2.infn.it (M. Salvato).

http://dx.doi.org/10.1016/j.carbon.2016.04.068
0008-6223/

systems such as sputtering. The result is a less expensive and faster way to fabricate networks of SNWs.

Taking advantage of the useful properties of CNTs, we deposited for the first time superconducting Nb on films of multiwall CNTs in order to obtain aggregates of Nb SNWs. Since Nb is the most studied among the superconducting elements and the most used in superconducting electronics, it represents the most suitable material to test new possible applications of the superconductivity at the nanoscale. We studied the transport properties of the resulting SNW aggregates for different Nb thickness ($d_{Nb}$) and compared the experimental results with those obtained on reference Nb thin films deposited on Si/$SiO_2$ substrates and with those expected for SNW networks. We found that when $d_{Nb}$ is reduced to the same order of the superconducting coherence length $\xi$, some interesting phenomena emerge in the SNW aggregates but not in the test reference films of the same thickness. These phenomena are related to phase slips (PS) [18,26,27] of the superconducting order parameter and they are peculiar of superconductors whose dimensions are of the order of nanometers. In particular, we observe thermally activated PSs (TAPS) that produce an increase of the electrical resistance of the SNWs at temperature $T$ just below the onset of the superconducting transition, $T_c^{on}$. This gives rise to a broadening of the resistive transitions with a consequent reduction of the zero resistance critical temperature $T_{c0}$ [19,28,29]. At lower temperatures and in thinner SNWs, quantum PS (QPS) processes cause the appearance of a tail in the resistive transition that inhibits superconductivity down to $T \rightarrow 0$ [30–33].

The paper is organized as follows. In Section 2 the experimental process for CNT and Nb deposition, together with the results of the morphological and compositional analysis, are presented. The superconducting and the normal state properties are shown in Sections 3 and 4 respectively, followed by the discussion of the experimental results in Section 5. Finally, Section 6 contains brief conclusions.

## 2. Experimental

Highly pure multiwall CNT powder (Nanocyl, NC3100, carbon purity >95%) was dispersed in aqueous solution (80 μg $mL^{-1}$) with 2% w/v sodium dodecyl sulfate (Sigma–Aldrich, assay >98.5%) anionic surfactant and tip-ultrasonicated (Branson S250A, 200 W, 20% power, 20 kHz) in an ice-bath for an hour. The unbundled supernatant was collected through a pipette and forms a well-dispersed suspension that remains stable for several months. Multiwall CNTs films were fabricated by a vacuum filtration process of 1 mL in volume of the dispersion cast on mixed cellulose ester filters (Pall GN6, 1 in diameter, 0.45 μm pore diameter). Subsequently, rinsing in water and in a solution of ethanol, methanol and water (15:15:70) was performed to remove as much surfactant as possible. Samples were made uniformly depositing by the dry-transfer printing method multiwall CNT films on Si/$SiO_2$ substrates. More details about this deposition technique without chemical deposition processes have been reported elsewhere [34]. Nanocyl transmission electron microscopy characterizations indicate a very small multiwall CNT average diameter $d_{CNT} \approx 9.5$ nm and an average length of 1.5 μm [35].

Nb layers with $d_{Nb}$ in the range 3–50 nm were deposited on CNT films by high-vacuum dc magnetron sputtering with a starting pressure in the low $10^{-8}$ mbar regime and in an $Ar^+$ deposition pressure of 4 μbar. The deposition rate was determined by X-ray reflectivity measurements on Nb films previously deposited on Si/$SiO_2$ substrates. All the samples were fabricated during the same deposition run in order to preserve the same growth conditions. A computer-controlled shutter was used to cover each sample after the required thickness was reached. Close to each CNT film, a Si/$SiO_2$ substrate was placed to obtain a reference Nb film of the same thickness. In what follows we name with CNTNb followed by a number indicating $d_{Nb}$ in nm, the aggregate of SNWs and with Nb, followed by the number corresponding to $d_{Nb}$, the reference Nb film. Transport properties were measured by using a standard d.c. four-probe technique in a $^4$He bath down to $T = 1.8$ K and a sorption pumped $^3$He HelioxVL insert from Oxford Instruments down to $T = 250$ mK. Van der Pauw four leads configuration [36] was used to measure the resistance vs. temperature ($R$–$T$) characteristics on a typical area of $2 \times 2$ $mm^2$ of the samples surface. In order to measure the current–voltage ($I$-$V$) characteristics, standard photolithographic technique was applied on a selection of CNT films for obtaining patterned samples. The photoresist was spanned on the whole CNT film and a strip 10 μm wide and with voltage contacts at a distance of 100 μm was developed. Then Nb was deposited on the whole surface and finally, by a standard lift-off procedure, a $10 \times 100$ $\mu m^2$ strip of SNW aggregates was obtained. In order to minimize the heating effects, $I$-$V$ curves were recorded by biasing the strip with a pulsed current (current-on time 12 ms, current-off time 1 s).

The inset in Fig. 1(a) schematically represents the morphology of each SNW. A layer of Nb with thickness $d_{Nb}$ covers the cylindrical surface of each CNT giving rise to the SNW. The cylindrical surface of the CNT is expected to give an oblong shape to the SNW (see the cross section in the lower part of the same inset) in the direction of the incoming sputtered species. The main panel of Fig. 1(a) shows a scanning electron microscope (SEM) micrograph of the SNWs corresponding to the sample CNTNb3. As sketched in the inset, the dot-ended line in the figure gives $d \approx d_{CNT} + 2d_{Nb}$, where $d_{CNT} = 9.5$ nm and, for this sample, $d_{Nb} = 3$ nm. A statistical analysis, performed by measuring the CNT diameter along the transverse direction on a large number of SNWs, returned $d = (15 \pm 2)$ nm which is consistent with the nominal values of $d_{CNT}$ and $d_{Nb}$.

The inset of Fig. 1(b) shows the compositional analysis of the sample CNTNb30 obtained by Electron Dispersive Spectroscopy. The presence of the Nb peak in the spectrum confirms its successful deposition on the CNT surface. C and Si peaks come from the CNTs and substrate, respectively, whereas the O peak arises mostly from the $SiO_2$ substrate surface layer and in part from $Nb_2O_5$ due to the oxidation of the Nb surface after its exposure to the atmosphere. The SEM micrograph of Fig. 1(b) shows the surface of the same sample. The statistical analysis of the available micrographs returns $d = (38 \pm 7)$ nm. The oblong shape of the SNWs, sharpened with respect to the CNTNb3 sample by the longer deposition time, is responsible for the discrepancy between this value and that expected by the expression $d \approx d_{CNT} + 2d_{Nb} = 69.5$ nm. Finally, the compact nature of the CNT film, as inferred by the SEM images, allows assuming that the electrical current flows between the electrical leads through each SNW and crosses the interfaces formed as contacts between them. The role of these interfaces and their influence on the transport properties of the aggregate will be discussed below.

Using the van der Pauw method, the resistivity was obtained for all the samples. In the case of the thicker sample (CNTNb50), from the measured low-temperature value of the resistivity, $\rho = 35$ μΩ cm, and from the relation $\rho\ell = 3.72 \times 10^{-6}$ μΩ $cm^2$ valid for Nb [37], a mean free path $\ell = 1.1$ nm was estimated. The Ginzburg-Landau coherence length $\xi(T) = \xi(0)/\sqrt{1 - T/T_c}$ and the magnetic field penetration depth $\lambda(T) = \lambda(0)/\sqrt{1 - T/T_c}$ can be found at any temperature using for $\xi(0)$ and $\lambda(0)$ the dirty limit expressions [38] (valid when $\ell < \xi_0$) $\xi(0) = 0.85\sqrt{\xi_0\ell}$ and $\lambda(0) = 0.66\lambda_0\sqrt{\xi_0/\ell}$ where $\xi_0 = 38$ nm and $\lambda_0 = 39$ nm [39] are the values for the BCS coherence length and London penetration depth of Nb, respectively. Therefore we obtain $\xi(0) = 6$ nm and $\lambda(0) = 151$ nm.

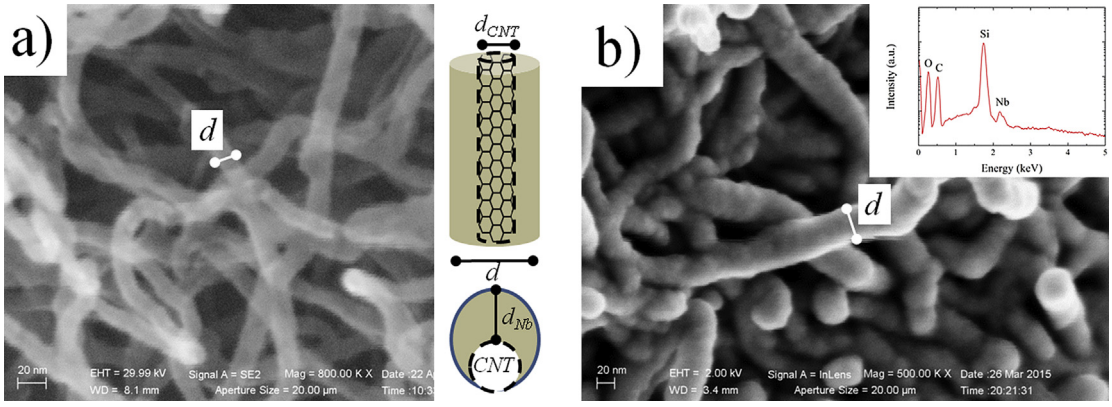


**Fig. 1.** a) SEM image of the sample CNTNb3. The dot-ended white line indicates the average diameter of a SNW. Inset: schematic of a SNW built using a CNT as a template (upper panel) and its cross section (lower panel); $d_{Nb}$, $d_{CNT}$ and $d$ represent the Nb thickness, the CNT diameter and the diameter of the whole structure, respectively. b) SEM image of the sample CNTNb30. The dot-ended line has the same meaning as in 1a. Inset: Energy Dispersive Spectrum of the same sample. (A color version of this figure can be viewed online.)

## 3. Superconducting properties

In Fig. 2 the $R-T$ transitions, in units of the quantum resistance $R_Q = h/4e^2 \cong 6.5k\Omega$ ($h$ is the Plank's constant and $e$ is the electron charge), are shown for the reference samples (Nb10-Nb50, Panel (a)) and for the Nb aggregates of SNWs (CNTNb10-CNTNb50, Panel (b)). While all the reference samples are superconducting with transition widths narrower than 0.1 K and with $R_N << R_Q$ ($R_N$ is the normal state resistance measured just before of the superconducting transition), the aggregates present different behavior, depending on $d_{Nb}$. The thicker samples (namely CNTNb50 and CNTNb40) show the same $T_c^{on}$ (defined as the temperature at which the resistance is reduced by 10% of the normal state resistance) of their reference Nb films and a finite but reduced $T_{c0}$, due to the large broadening of the $R-T$ curves. Decreasing $d_{Nb}$, $T_c^{on}$ remains finite, while full superconducting behavior is inhibited down to the lowest measured temperature ($T = 250$ mK) as observed for the samples CNTNb30 and CNTNb20. Finally, the sample with the thinnest Nb layer, CNTNb10, presents a semiconducting behavior without any trace of superconductivity. The same dependence is observed for aggregates of Nb SNWs with $d_{Nb}$<10 nm. Moreover, it is worth noticing that all the aggregates that present a finite $T_c^{on}$ have $R_N \leq R_Q$ while the samples with $R_N > R_Q$ show a semiconducting behavior down to the lowest temperature. This suggests the presence of a superconductor-insulator (S-I) transition with decreasing $d_{Nb}$ with $R_N \cong R_Q$ as a crossover resistance. This result, observed in many low dimensional materials [40,41] as well as in SNWs [42,43], found many controversial explanations [41]. In the case of SNWs it is interpreted in terms of charge localization [42], or as due to local magnetic moments present in the wire [44]. Other mechanisms such as, for example, electron interactions with surface phonons [45], invoked as possible cause of the reduction of $T_c$ [46] and of the S-I transition [41] in low dimensional systems, can be ruled out in our case. In fact, being the $T_c^{on}$ of the aggregates of SNWs and of the reference films the same, the electron-phonon (e-ph) coupling constant in these systems should also be the same. Therefore, the S-I transition should be ascribed to other causes. A more intriguing explanation concerns the nature of weak link constrictions (WLCs) present inside a single polycrystalline SNW at the interfaces between the grains. In this case, the insulating or metallic nature of the WLCs determines if $R_N > R_Q$ or $R_N < R_Q$ [25,43]. Here, the hypothesis of the WLC at the base of the appearance of the S-I transition seems to be the most appropriate due to the large number of interfaces present in our systems. In fact, for low values of $d_{Nb}$, the weak coupling between the interfaces is favored with the consequent development of the S-I transition.

For a deeper understanding of the nature of the superconducting transitions, the $R-T$ curves were fitted by using the

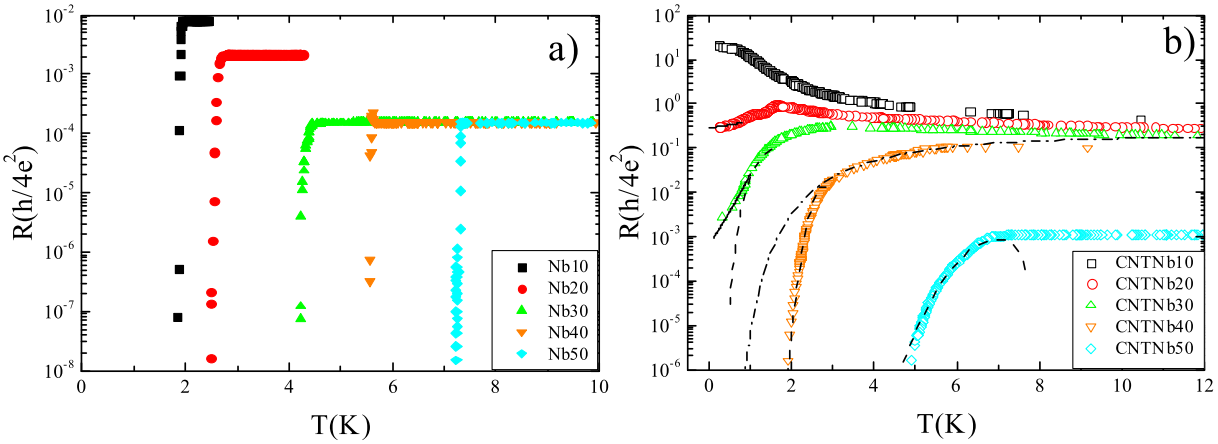


**Fig. 2.** Resistance in units of quantum resistance as a function of $T$ for (a) the Nb reference samples and (b) the SNW aggregates. The lines in the right panel are fits to the data using the TAPS model (Eq. (1)-dashed lines), QPS model (Eq. (2)-solid lines) and Ambegaokar-Halperin (AH) model (dot-dashed line for CNTNb40). (A color version of this figure can be viewed online.)

expressions for the TAPS and QPS models. In particular, the data corresponding to CNTNb50, CNTNb40 and, just below $T_c^{on}$, to CNTNb30 were fitted by the expression, valid in TAPS regime for an individual SNW [47]:

$$R_{TAPS} = \frac{16\sqrt{6}}{\pi^{2/3}} R_Q \frac{L}{\xi(T)} \frac{T^*}{T} \sqrt{\frac{U(T)}{k_B T}} \exp\left[-\frac{U(T)}{k_B T}\right] \quad (1)$$

where $k_B$ is the Boltzmann constant, $T^* \cong T_c^{on}$ [19] and $U(T) = U(0)(1 - T/T_c)^{3/2}$ is the temperature dependent PS activation energy. Here $\xi(0) = 6$ nm, as measured for our Nb films [22,23], and $L$, which in the TAPS model represents the length of an individual SNW, is treated as a fitting parameter together with $U(0)$ [22,23]. The best fitting processes obtained with $L = 62$ nm, 56 nm, 57 nm and $U(0) = 179.5$ K, 111.9 K, 8.3 K for CNTNb50, CNTNb40 and CNTNb30 respectively, are reported as dashed lines in Fig. 2(b). It results that $U(0) > k_B T$ as expected for activation energy and as observed in other template SNW networks [21]. Particular attention should be devoted to the parameter $L$ that in the models represents the length of an individual SNW, but that is not a well-defined quantity in the case of network of SNWs [21]. Indeed, Eq. (1) describes TAPS mechanisms inside an individual SNW and it cannot be rigorously applied to aggregates of SNWs. However, Eq. (1) was also used in the case of network of SNWs [21–23] where $L$ assumes an arbitrary meaning as the length of a single unit of the network or the distance between the electric contacts. In our case, we obtain $L = 56$–$62$ nm, values which are roughly of the same order of the length of a single CNT inside the template film as shown in Fig. 1(b).

While the TAPS model satisfactory reproduces the whole $R$–$T$ curves for the samples CNTNb50 and CNTNb40, only the high temperature part of the resistive transition of the sample CNTNb30 is nicely reproduced by Eq. (1). The tail appearing at low temperatures deviates from the TAPS behavior and extrapolates to a finite resistance value at $T = 0$. At low temperatures, TAPS effects are negligible and such tails can be due to the appearance of quantum phenomena. Following these statements, we fitted the tail of the $R$–$T$ data of the sample CNTNb30 using the expression [48,49]:

$$R_{QPS} \cong AB \frac{R_Q^2}{R_N} \frac{L^2}{\xi_0^2} \exp\left[-A \frac{R_Q}{R_N} \frac{L}{\xi(T)}\right] \quad (2)$$

valid for QPS where $A$, $B$ and $L$ are used as adjustable parameters. The same expression was used to fit the low temperature part of the resistive transition of the sample CNTNb20. For both the samples CNTNb30 and CNTNb20 we obtained $L = 57$ nm ($A = 0.21$ K$^{-1}$ and $B = 1.33$ K for CNTNb30, $A = 0.20$ K$^{-1}$ and $B = 0.53$ K for CNTNb20). These results are shown in Fig. 2(b). For thinner Nb thickness, as already stated, no superconducting onset transition was observed.

The presence of PS is also evidenced in the $I$-$V$ characteristics measured on bridges of SNW aggregates. In the lower inset of Fig. 3 the $I$-$V$ characteristics of the patterned sample CNTNb40 in the temperature range $T = 4.0$ K–4.4 K is shown. Non-linearity and voltage steps are present at low temperatures, while hysteresis is absent in all the investigated temperature range. Increasing the temperature, an evolution towards the Ohmic behavior is observed with disappearance of the voltage steps. The main panel of Fig. 3 shows the low current part of the $I$-$V$ curves reported in the inset. All the $I$-$V$ characteristics show the presence of a finite resistance as expected for TAPS. Indeed, all the experimental data can be reproduced by the expression [27,47]:

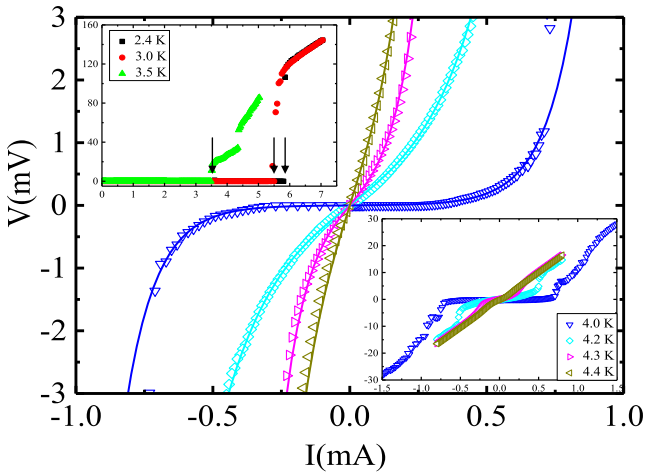


**Fig. 3.** $IV$ characteristics at different temperatures for the patterned CNTNb40 sample, $T = 4.0$ K, 4.2 K, 4.3 K, and 4.4 K. The lines are fit to the data obtained using Eq. (3). Lower inset: same of the main panel but in an extended range. Upper inset: $IV$ characteristics of the same sample at lower temperatures. For the insets, the axes units are the same as in the main panel. (A color version of this figure can be viewed online.)

$$V \propto \sinh\left(\frac{I}{I_0}\right) \quad (3)$$

valid in the TAPS regime, where $I_0$ was treated as a fitting parameter. The best fit to the data is obtained for $I_0 \approx 0.1$ μA, in quite good agreement with the expected value $I_0 = 2ek_BT/\pi\hbar = 0.06$ μA [27,47] and in perfect agreement with the same value obtained in the case of isolated SNW templated by CNT [50]. The voltage steps in the non-linear part of the $I$-$VI$ characteristics are enhanced as the temperature is further reduced as shown in the upper inset of Fig. 3, where the $I$-$V$ measurements are reported for T < 4.0 K. In this temperature range, the transition to the normal state is stepwise with a large voltage step at the critical current $I_c$, indicated by arrows in the figure, and a series of minor jumps. The jumpwise increase of the voltage is commonly observed in the case of both individual and networks of SNWs and is ascribed to the presence of PS centers [25,43].

Assuming a homogeneous strip with section 40 nm × 10 μm, a critical current density $J_c = 1.5 \cdot 10^6$ A/cm$^2$ at the lowest measured temperature $T = 2.4$ K is obtained. This value gives a depairing critical current density $J_{dp} = 3\sqrt{3}J_c/2 = 4 \cdot 10^6$A/cm$^2$ which is of the same order of that found in other templated SNW systems [22] and about one order of magnitude lower than the one evaluated in the framework of the model of Kupriyanov and Lukichev (KL) [51] which gives $J_{dp}^{KL} = 3.5 \cdot 10^7$A/cm$^2$. This discrepancy can be ascribed to the rough estimation made for $J_c$ in assuming a uniform Nb strip. Indeed, the SNW aggregate, even compactly confined in a strip, presents a reduced cross section given by the sum of the cross sections of each SNW. On the other hand, to estimate the number of the SNWs inside the strip is a difficult task and the precise determination of the $J_c$ value would not add any further information to the discussion. However, the high value obtained for $J_c$ confirms that overheating effects are negligible and that the heating due to the contact leads made on the SNW aggregates is satisfactory shunted by the CNT film.

## 4. Normal state properties

The nucleation of superconductivity in the SNW aggregates can be related to some of their electric transport properties in the

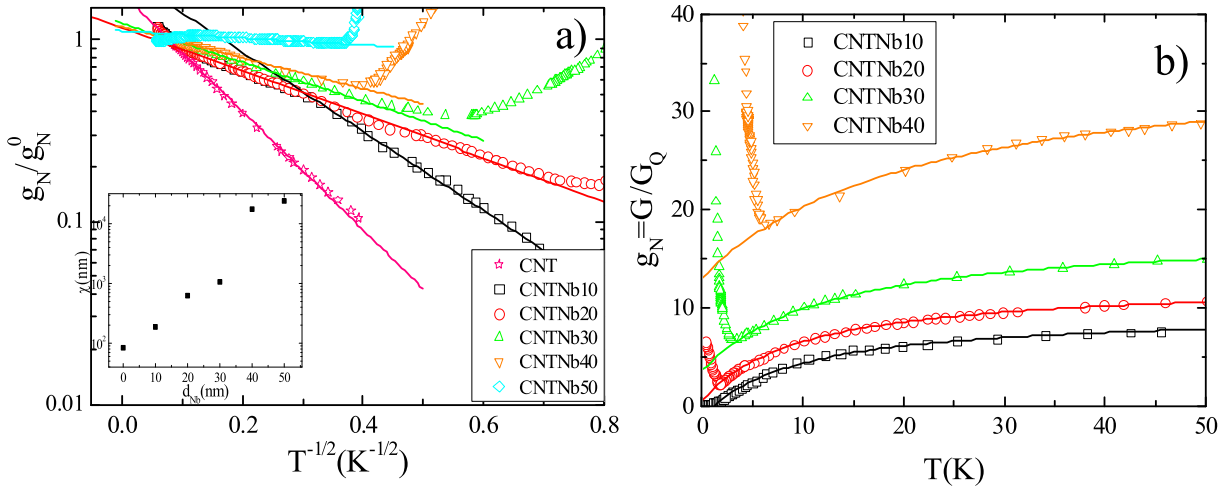


**Fig. 4.** a): Conductance normalized with respect to its value at $T = 150$ K, vs. $1/\sqrt{T}$. The lines are fit to the data using Eq. (4). Inset: electron localization length $\chi$ vs. $d_{Nb}$. -b): Temperature dependence of the normalized conductance. The lines are the best fit to the data obtained according to the diffusive Coulomb blockade model, Eq. (5). (A color version of this figure can be viewed online.)

normal state. The SEM images evidenced a disordered structure formed by SNWs connected by surface contacts to form the aggregate. For this kind of systems, co-tunneling effects and Coulomb blockade mechanism are commonly evoked to explain the transport properties in the normal state [52,53]. In these models, the electrons are confined within a localization length $\chi$ and move across the disordered system tunneling through the Coulomb barrier. At low bias, the temperature dependence of the normalized conductance $g_N = G/G_Q$, where $G = 1/R$ and $G_Q = 2e^2/h$, is the same as that expressed by the Efros-Shklovskii model [54] of variable range hopping:

$$g_N = g_N^0 e^{-\sqrt{T_0/T}} \tag{4}$$

Here $g_N^0$ is a normalization constant and $T_0 = 2.8e^2/4\pi\varepsilon_0\varepsilon k_B\chi$ [52,53] is a characteristic temperature. Fig. 4(a) shows $g_N$, normalized with respect to the value at $T = 150$ K, as a function of $1/\sqrt{T}$ in semilogarithmic scale. The experimental data follow a straight line from $T = 150$ K down to $T_c^{on}$, and they are well approximated by expression (4), where $T_0$ has been left as the only adjustable parameter. The inset of Fig. 4(a) shows the $\chi$ vs. $d_{Nb}$ dependence extracted from the expression of $T_0$ where we have used the values $\varepsilon_0$=8.85 $\times$ $10^{-12}$ F/m and $\varepsilon = 10$ [55] for the permittivity of the free space and Nb, respectively. The high values of $\chi$ compared to the length of the SNWs shown in Fig. 1 indicate that electrons are localized on distances much longer than the length of the single SNW in the aggregate. This suggests that the interface barriers do not substantially affect the motion of the charge carriers along the whole aggregate and leads to consider that a different diffusive transport mechanism could be the precursor of the superconductivity in our samples. If a Coulomb blockade mechanism is responsible for current transport [56], the sample conductance is given by

$$\frac{G_0}{G_0 - G(T)} \cong \frac{3k_BT}{\beta E_c} \tag{5}$$

where $\beta = 1/3$. Fig. 4(b) shows the experimental data together with the fit obtained using the expression (5) in which $E_c$ is left as the only free parameter. For the sake of clarity, we have not plotted data of the sample CNTNb50. The fits are very good indicating diffusive Coulomb blockade as a possible mechanism for $T > T_c^{on}$, as also supported by the low values obtained for $E_c$ that are less than 1 meV for all the analyzed samples. The same Coulomb blockade mechanism was previously invoked to study the current transport in isolated MoGe SNWs templated by CNTs [56].

## 5. Discussion

The analysis of the normal state properties of the SNW aggregates confirms the experimental evidence of the presence of TAPS and QPS in the superconducting state. The long electron localization lengths indicate that the characteristic distances are much longer than the single CNT exposed to the Nb deposition and that interface contacts between two different SNWs do not considerably affect the superconducting properties. On the other hand, in the superconducting state, the interfaces between different SNWs could also be considered as WLCs where Josephson effect instead of PS can take place. Discerning between these two phenomena using transport measurements is a difficult task even in an isolated SNW, because WLCs formed between not detectable grains can be present and they can be considered as PS centers [22–28,43,57]. In the case of the networks, the interfaces between different SNW can play the same role of PS centers. In order to understand whether Josephson effect was present in our networks we tried to fit the resistive transitions shown in Fig. 2(b) with the Ambegaokar-Halperin (A-H) expression for JJs [58]. For the sake of clarity, only the fit to the data of the CNTNb40 sample is reported in the figure (dot-dashed line). The fit appears to be very poor if compared with the one obtained using the TAPS expression.

Another argument suggesting the presence of PS in the analyzed samples is the $R_Q$ crossover of the S-I transition which was observed in homogeneous isolated SNW [25,43,44] as well as in arrays of SNWs [59] where QPS are present. In these systems, the S-I transition crossover does depend on the value of $R_N$ and on the length of the SNW (measured with respect to $\xi$). In particular, following Ref. [59] QPS emerge in 2D-arrays of SNWs when the ratio between the PS energy $E_S$ and inductive energy $E_L$:

$$\frac{E_S}{E_L} = \frac{a}{17.4}\frac{L^2}{\xi^2}e^{-B\frac{L}{\xi}\frac{R_Q}{R_N}} = \alpha_c \tag{6}$$

increases above the critical value $\alpha_c = 0.051$. In this expression, $B$ is the same constant present into Eq. (2). From Eq. (6) one can

straightforwardly obtain an expression for the ratio $R_N/R_Q$:

$$\frac{R_N}{R_Q} = \frac{L}{\xi}\frac{B}{\ln\left(\left(\frac{L}{\xi}\right)^2 c\right)} \quad (7)$$

where $c = a/17.4\alpha_c$. This last expression relates the normalized resistance $R_N/R_Q$ to the normalized length $L/\xi$ through the constants $B$ and $c$ that have to be determined by the experimental data. Using $B = 0.079$, as obtained from the fitting of the $R-T$ curve of the sample CNTNb20 in Fig. 2(b), and $c = 0.05$ as suggested in [59], the value $R_N/R_Q \approx 0.91$ is obtained at the S-I crossover. This value is in very good agreement with the results reported in Fig. 2(b) where the crossover for the S-I transition takes place at $R_N \cong R_Q$. The model proposed in [59] refers to arrays of SNWs where QPS instead of Josephson effects governs the transport mechanism in the superconducting state. The obtained result further confirms that QPS events are dominant and that the WLCs at the interfaces eventually behave as PS center instead of JJs in the analyzed SNW aggregates.

## 6. Conclusions

We reported on superconducting and normal state properties of aggregates of SNWs obtained by sputtering Nb on CNT films deposited by dry-transfer printing on $Si/SiO_2$ substrates. The charge transport mechanism in the normal state is characterized by diffusive Coulomb Blockade which is also observed in both isolated and in arrays of SNWs showing a S-I transition. All the samples with a finite $T_c^{on}$ show the presence of PS in the superconducting state that have a thermal (quantum) nature in the case of thicker (thinner) SNWs. All the evidenced effects are common in SNW obtained by other techniques and confirm that CNT films can be used to obtain networks of SNWs. The accessible and not expensive method adopted here opens new perspectives on the possibility to use CNT films as one-dimensional interconnect in the field of superconducting nanoelectronics.

## Acknowledgments

PC, MDC and MS thank the European Community for the RISE Project CoExAN GA644076.

## References

[1] Nanotubes and nanowires, University of California, Irvine, USA, in: P.J. Burke (Ed.), Selected Topics in Electronic Systems, vol. 44World Scientific Publishing, Singapore, 2007. ISBN-13 978-981-270-453-1.
[2] T. Zhang, S. Mubeen, N.V. Myung, M.A. Deshusses, Recent progress in carbon nanotube-based gas sensors, Nanotechnology 19 (2008) 332001–332014.
[3] P. Castrucci, Carbon nanotube/silicon hybrid heterojunctions for photovoltaic devices, Adv. Nano Res. 2 (1) (2014) 23–56.
[4] M. Salvato, M. Lucci, I. Ottaviani, M. Cirillo, E. Tamburri, I. Cianchetta, et al., Effect of potassium doping on electrical properties of carbon nanotube fibers, Phys. Rev. B 84 (23) (2011) 2334061–2334063.
[5] M.S. Raghuveer, A. Kumar, M.J. Frederick, G.P. Louie, P.G. Ganesan, G. Ramanath, Site-selective functionalization of carbon nanotubes, Adv. Mater. 18 (2006) 547–552.
[6] M. Scarselli, L. Camilli, L. Matthes, O. Pulci, P. Castrucci, E. Gatto, et al., Photoresponse from noble metal nanoparticles-multi walled carbon nanotube composites, Appl. Phys. Lett. 101 (24) (2012) 2411131–2411134.
[7] M. Scarselli, L. Camilli, P. Castrucci, F. Nanni, S. Del Gobbo, E. Gautron, et al., In situ formation of noble metal nanoparticles on multiwalled carbon nanotubes and its implication in metal-nanotube interactions, Carbon 50 (2012) 875–884.
[8] Y. Zhang, H. Dai, Formation of metal nanowires on suspended single-walled carbon nanotubes, Appl. Phys. Lett. 77 (19) (2000) 3015–3017.
[9] A. Bezryadin, A. Bollinger, D. Hopkins, M. Murphey, M. Remeika, A. Rogachev, Superconducting nanowires template by single molecules, in: Encyclopedia of Nanoscience and Nanotechnology, Dekker, New York, 2010, pp. 3761–3773, http://dx.doi.org/10.1081/E-ENN 120013540.
[10] J. Hone, M.C. Llaguno, N.M. Nemes, A.T. Johnson, J.E. Fischer, et al., Electrical and thermal transport properties of magnetically aligned single wall carbon nanotube films, Appl. Phys. Lett. 77 (5) (2000) 666–668.
[11] J.E. Mooij, YuV. Nazarov, Superconducting nanowires as quantum phase-slip junctions, Nat. Phys. 2 (2006) 169–172.
[12] A. Johansson, G. Sambandamurthy, D. Shahar, N. Jacobson, R. Tenne, Nanowire acting as a superconducting quantum interference device, Phys. Rev. Lett. 95 (2005), 116805–1-4.
[13] A. Falk, M.M. Deshmukh, A.L. Prieto, J.J. Urban, A. Jonas, H. Park, Magnetic switching of phase-slip dissipation in NbSe2 nanoribbons, Phys. Rev. B 75 (2) (2007) 0205011–0205014.
[14] C.H. Webster, J.C. Fenton, T.T. Hongisto, S.P. Giblin, A.B. Zorin, P.A. Warburton, NbSi nanowire quantum phase-slip circuits: dc supercurrent blockade, microwave measurements, and thermal analysis, Phys. Rev. B 87 (14) (2013) 1445101–14451012.
[15] O.V. Astafiev, L.B. Ioffe, S. Kafanov, Y.A. Pashkin, K.Y. Arutyunov, D. Shahar, et al., Coherent quantum phase slip, Nature 484 (2012) 355–358.
[16] J.E. Moij, C.J.P.M. Harmans, Phase-slip flux qubits, New J. Phys. 7 (2005) 2191–2197.
[17] J. Ku, V. Manucharyan, A. Bezryadin, Superconducting nanowires as nonlinear inductive elements for qubits, Phys. Rev. B 82 (13) (2010) 1345181–13451811.
[18] R. Fazio, H. van der Zant, Quantum phase transitions and vortex dynamics in superconducting networks, Phys. Rep. 355 (2001) 235–334.
[19] H.S.J. van der Zant, M.N. Webster, J. Romijn, J.E. Mooij, Vortices in two dimensional superconducting weakly coupled wire networks, Phys. Rev. B 50 (1) (1994) 340–350.
[20] W.J. Zhang, S.K. He, H. Xiao, G.M. Xue, Z.C. Wen, X.F. Han, et al., Transport measurements on nano-engineered two dimensional superconducting wire networks, Phys. C 480 (2012) 126–128.
[21] Q. Luo, X.Q. Zeng, M.E. Miszczak, Z.L. Xiao, J. Pearson, T. Xu, et al., Phase slippage driven dissipation and high-field Little-Parks effect in superconducting MoGe nanowire networks formed on nanoporous substrates, Phys. Rev. B 85 (17) (2012) 1745131–1745137.
[22] C. Cirillo, M. Trezza, F. Chiarella, A. Vecchione, V.P. Bondarenko, S.L. Prischepa, et al., Quantum phase slips in superconducting Nb nanowire networks deposited on self-assembled Si templates, Appl. Phys. Lett. 101 (17) (2012) 1726011–1726015.
[23] M. Trezza, C. Cirillo, P. Sabatino, G. Carapella, S.L. Prischepa, C. Attanasio, Nonlinear current-voltage characteristics due to quantum tunneling of phase slips in superconducting Nb nanowire networks, Appl. Phys. Lett. 103 (25) (2013) 2526011–2526014.
[24] K. Xu, J.R. Heath, Long, highly-ordered high-temperature superconductor nanowire arrays, Nano Lett. 8 (11) (2008) 3845–3849.
[25] K. Xu, J.R. Heath, Controlled fabrication and electrical properties of long quasi-one-dimensional superconducting nanowire arrays, Nano Lett. 8 (1) (2008) 136–141.
[26] A. Bezryadin, Quantum suppression of superconductivity in nanowires, J. Phys. Condens. Matter 20 (2008) 0432021–04320219.
[27] K.Y. Arutyunov, D.S. Golubev, A.D. Zaikin, Superconductivity in one dimension, Phys. Rep. 464 (2008) 1–70.
[28] M. Zgirski, K.Y. Arutyunov, Experimental limits of the observation of thermally activated phase-slip mechanism in superconducting nanowires, Phys. Rev. B 75 (17) (2007) 1725091–1725094.
[29] A. Rogachev, A.T. Bollinger, A. Bezryadin, Influence of high magnetic fields on the superconducting transition of one-dimensional Nb and MoGe nanowires, Phys. Rev. Lett. 94 (1) (2005) 0170041–0170044.
[30] N. Giordano, Evidence for macroscopic quantum tunneling in one-dimensional superconductors, Phys. Rev. Lett. 61 (18) (1988) 2137–2140.
[31] C.N. Lau, N. Markovic, M. Bockrath, A. Bezryadin, M. Tinkham, Quantum phase slips in superconducting nanowires, Phys. Rev. Lett. 87 (21) (2001) 2170031–2170034.
[32] N. Giordano, E.R. Schuler, Macroscopic quantum tunneling and related effects in a one-dimensional superconductor, Phys. Rev. Lett. 63 (21) (1989) 2417–2420.
[33] F. Altomare, A.M. Chang, M.R. Melloch, Y. Hong, C.W. Tu, Evidence for macroscopic quantum tunneling of phase slips in long one-dimensional superconducting Al wires, Phys. Rev. Lett. 97 (1) (2006) 0170011–0170014.
[34] F. De Nicola, P. Castrucci, M. Scarselli, F. Nanni, I. Cacciotti, M. De Crescenzi, Multi-Fractal Hierarchy of single-walled carbon nanotube hydrophobic coatings, Sci. Rep. 5 (2015) 85831–85839.
[35] http://www.nanocyl.com/en/Products-Solutions/Products/Research-Grades/Thin-Multi-Wall-Carbon-Nanotubes.
[36] L.J. van der Pauw, A method of measuring specific resistivity and Hall effect of discs of asbitrary shape, Philips Res. Rep. 13 (1958) 1–9.
[37] M.S.M. Minhaj, S. Meepagala, J.T. Chen, L.E. Wenger, Thickness dependence on the superconducting properties of thin Nb films, Phys. Rev. B 49 (1994) 15235–15240.
[38] C. Strunk, V. Bruyndoncx, V.V. Moshchalkov, C. Van Haesendonck, Y. Bruynseraede, R. Jonckheere, Nonlocal effects in mesoscopic superconducting aluminum structures, Phys. Rev. B 54 (1996) R12701–R12704.
[39] B.W. Maxfield, W.L. McLean, Superconducting penetration depth of niobium, Phys. Rev. 139 (1965) A1515–A1522.
[40] A. Bezryadin, Superconductivity in Nanowires, Wiley-VCH Verlag GmbH & Co KGaA, Singapore, 2013, ISBN 978-3-527-40832-0.

[41] Yen-Hsiang Lin, J. Nelson, A.M. Goldman, Superconductivity of very thin films: the superconductor-insulator transition, Phys. C 514 (2015) 130–141.
[42] H. Kim, S. Jamali, A. Rogachev, Superconductor-insulator transition in long MoGe nanowires, Phys. Rev. Lett. 109 (2) (2012) 0270021–0270025.
[43] A.T. Bollinger, A. Rogachev, M. Remeika, A. Bezryadin, Effect of morphology on the superconductor-insulator transition in one-dimensional nanowires, Phys. Rev. B 69 (18) (2004) 1805031–1805034.
[44] A.T. Bollinger, R.C. Dinsmore III, A. Rogachev, A. Bezryadin, Determination of the superconductor-insulator phase diagram for one-dimensional wires, Phys. Rev. Lett. 101 (22) (2008) 2270031–2270034.
[45] J.M. Dickey, A. Paskin, Phonon spectrum in small particles and their implications for superconductivity, Phys. Rev. Lett. 21 (20) (1968) 1441–1443.
[46] W.L. McMillan, Transition temperature of strong-coupled superconductors, Phys. Rev. 167 (2) (1968) 331–334.
[47] D.S. Golubev, A.D. Zaikin, Thermally activated phase slips in superconducting nanowires, Phys. Rev. B 78 (14) (2008) 1445021–1445028.
[48] A.D. Zaikin, D.S. Golubev, A. van Otterlo, G.T. Zimanyi, Quantum phase slips and transport in ultrathin superconducting wires, Phys. Rev. Lett. 78 (8) (1997) 1552–1555.
[49] D.S. Golubev, A.D. Zaikin, Quantum tunneling of the order parameter in superconducting nanowires, Phys. Rev. B 64 (1) (2001) 014504–0145014.
[50] A. Rogachev, A. Bezryadin, Superconducting properties of polycrystalline Nb nanowires template by carbon nanotubes, Appl. Phys. Lett. 83 (3) (2003) 512–514.
[51] M.Y. Kupriyanov, K.K. Likharev, V.F. Lukichev, Influence of effective electron interaction on the critical current in Josephson weak links, Zh Eksp. Teor. Fiz. 83 (1982) 431–441.
[52] T.B. Tran, I.S. Beloborodov, J. Hu, X.M. Lin, T.F. Rosenbaum, H.M. Jaeger, Sequential tunneling and inelastic cotunneling in nanoparticle arrays, Phys. Rev. B 78 (7) (2008) 0754371–0754379.
[53] T.B. Tran, I.S. Beloborodov, X.M. Lin, T.P. Bigioni, V.M. Vinokur, H.M. Jaeger, Multiple cotunneling in large quantum dot arrays, Phys. Rev. Lett. 95 (7) (2005) 0768061–0768064.
[54] B.I. Shklovskii, A.L. Efros, Electronic Properties of Doped Semiconductors, Springer, Berlin, 1984.
[55] A.I. Golovashkin, I.E. Leksina, G.P. Motulevich, A.A. Shubin, The optical properties of Nb, Sov. Phys. JETP 29 (1) (1969) 27–34.
[56] A.T. Bollinger, A. Rogachev, A. Bezryadin, Dichotomy in short superconducting nanowires: thermal phase slippage vs. Coulomb blockade, Europhys. Lett. 76 (3) (2006) 505–511.
[57] S.L. Chu, A.T. Bollinger, A. Bezryadin, Phase slips in superconducting films with constrictions, Phys. Rev. B 70 (21) (2004) 2145061–2145066.
[58] V. Ambegaokar, B.I. Halperin, Voltage due to thermal noise in the dc Josephson effect, Phys. Rev. Lett. 22 (25) (1969) 1364–1366.
[59] J.E. Mooij, G. Schon, A. Shnirman, T. Fuse, C.J.P.M. Harmans, H. Rotzinger, et al., Superconductor-insulator transition in nanowires and nanowire arrays, New J Phys. 17 (2015) 033006.